Flow Measurement and Instrumentation xxx (xxxx) xxx–xxx

Contents lists available at ScienceDirect

Flow Measurement and Instrumentation

journal homepage: www.elsevier.com/locate/flowmeasinst

Solid motion in a three-phase bubble column examined with Radioactive Particle Tracking

Gabriel Salierno[a], Mauricio Maestri[a], Stella Piovano[a], Miryan Cassanello[a,*], María Angélica Cardona[b], Daniel Hojman[b], Héctor Somacal[b,c]

[a] Laboratorio de Reactores y Sistemas para la Industria–LARSI, Dep. Industrias, FCEyN, Universidad de Buenos Aires, Intendente Güiraldes 2620, C1428BGA Buenos Aires, Argentina
[b] Laboratorio de Diagnóstico por Radiaciones–LADiR, Dep. Física Experimental, Comisión Nacional de Energía Atómica (CNEA), San Martín, Buenos Aires, Argentina
[c] Escuela de Ciencia y Tecnología, Universidad Nacional de San Martín, Buenos Aires, Argentina

ARTICLE INFO

Keywords:
Axially aligned detectors
Radioactive Particle Tracking
Solid motion
Three-phase bubble column

ABSTRACT

Radioactive Particle Tracking (RPT) is a powerful advanced technique for studying the solid motion within industrial scale multiphase reactors. However, it is rather difficult to implement in actual industrial installations, mainly due to the required calibration stage under actual operating conditions. This work has the aim of comparing the motion of calcium alginate beads in a three-phase bubble column examined either with RPT or with an array of the same scintillation detectors used for RPT, but located vertically aligned beside the analyzed vessel. Liquid and solid used for the experiments were in batch mode and mixed by circulating air. The homogeneous and heterogeneous regimes have been explored. Results arising from both techniques, like axial tracer trajectories, axial profiles of tracer positions probabilities, solid axial mixing times and solid axial dispersion coefficients are compared, for highlighting the relevant information that can be extracted from the simplified method, validated by RPT. It is found that the simplified method fairly coincides with the classic technique for estimating several relevant parameters. Finally, the estimated flow regime transition inferred from the simplified method by symbolic analysis is compared with the one arising from chordal holdup trends determined by gamma densitometry, also with satisfactory agreement.

1. Introduction

Three-phase bubble columns and fluidized bed reactors are used for many operations and processes of the chemical and related industries [1,2]. Fermentations that require biomass agglomerates or immobilized microorganisms, some of them intended for effluent treatments [3], or Fisher-Tropsch process [4] that produces liquid fuels from natural gas by a gas-liquid-solid catalytic reaction are examples of applications in diverse fields.

Proper design, optimization and monitoring of industrial scale units preferentially require knowledge of solid motion and distribution within the vessels [5]. In addition, for validation of granular dynamics simulations, experimental data of the solid motion is essential [6,7]. Industrial equipments have usually opaque walls and multiphase systems themselves are inherently opaque. Consequently, techniques that exploit interaction of the system with visible light have limited applications; high-energy radiation is more appropriate for obtaining information about the phases' behavior in multiphase systems [8,9].

Radioactive Particle Tracking (RPT) is an advanced metrology technique which allows capturing the actual path of a flow follower freely moving in a 3D environment [10]. It has been successfully applied to study many different multiphase reactors [8–24]. Part of the information arising from RPT is related to the analysis of the tracer axial trajectory, and especially when the tracer undergoes fast ascending paths [21–23]. A rapid and non-invasive diagnosis of macroscopic mixing, of potential use in monitoring of an operating reactor is desirable in the industry. RPT has proved very useful for diagnosing solid mixing in three-phase fluidized beds [24].

Even if RPT provides a complete panorama of the examined vessel and thorough information of the solid mixing, its use for industrial units is rather complicate, mainly due to the required calibration stage under actual operating conditions. This work is intended to evidence the ability of a simplified version of RPT, which does not require the calibration stage, to provide key information of the solid mixing and other relevant parameters. The motion of calcium alginate beads in a three-phase bubble column operating with liquid and solid in batch and

* Corresponding author.
E-mail address: miryan@di.fcen.uba.ar (M. Cassanello).

http://dx.doi.org/10.1016/j.flowmeasinst.2017.10.002
Received 31 January 2017; Received in revised form 27 June 2017; Accepted 5 October 2017

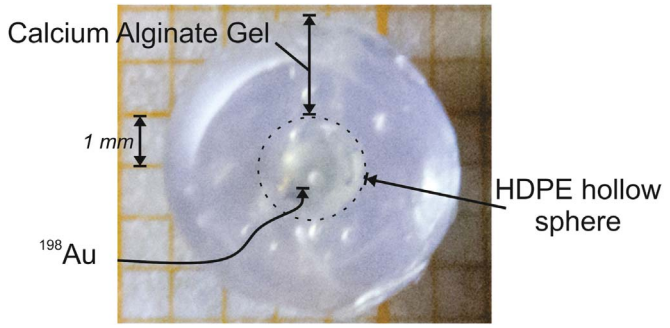

Fig. 1. Coated ^{198}Au tracer representing alginate beads.

different gas velocities is studied. RPT is applied for reconstructing the 3D trajectory of a radioactive tracer with the same features as the other calcium alginate beads, from which relevant information is extracted. In addition, a simplified version of RPT using the same scintillation detectors located axially aligned beside the analyzed vessel (RPT-AAD) is applied to get the tracer axial trajectory. Results arising from RPT-AAD are compared to those from RPT to highlight the capabilities and limitations of the simplified method. The ability of the simplified version to provide key information of the solid mixing in the given system in spite of the limited spatial resolution is evidenced.

2. Experimental section

Experiments have been carried out in a 1.2 m high and 0.1 m inner diameter acrylic column. Liquid and solid were in batch mode and mixed by circulating air. The model liquid used was a 0.5 M $CaCl_2$ aqueous solution with added benzalkonium chloride (0.1 ppm) both as fungicide and to promote foam formation. The solid inventory, calcium alginate beads of 5 mm mean diameter, were prepared by dropping a 1.5% (w/v) sodium alginate aqueous solution onto a 0.5 M $CaCl_2$ solution using a peristaltic pump, to form the calcium alginate beads by ion exchange. Density of the liquid and the solid were very similar: 1018 kg/m^3 and 1025 kg/m^3, respectively. The solid inventory represented 10% v/v of the fed liquid. The solid-liquid mixture height at rest was 0.55 m. Gas superficial velocity was varied within the range of 0.01–0.13 m/s.

Special care was taken to prepare the tracer used to track the solid, so as to match the size and density and also the texture and wettability of the suspended gel particles. For this purpose, a high density polyethylene (HDPE) bead containing a tiny piece of gold was embedded in an alginate bead similar to the rest of the particles in the bed (Fig. 1). The gold embedded in HDPE was previously activated by neutron bombardment in the RA1 reactor of the National Commission of Atomic Energy in Argentina (CNEA), giving ^{198}Au ($t_{1/2}$ = 2.7d, E_{peak} = 412 keV) of around 50 μCi. Gold 197 has a high neutron capture cross section [25], which allows using only a few micrograms and a moderate exposure to neutron bombardment to obtain appropriate activities for performing RPT experiments in the examined facility. In addition, it is easy to manipulate, highly insoluble in the system media, and it has a relatively short lifetime, which is relevant to the safety of the method.

The already activated tracer was then deposited inside matrices of half spheres designed for producing the alginate bead tracer in three steps; the resulting tracer was similar to the calcium alginate beads forming the bed. Further details on the preparation method can be found in [26].

Two arrangements of detectors have been used, as observed in the pictures shown in Fig. 2.

For RPT method, the motion of the radioactive tracer, representing the alginate beads, was continuously followed (every 30 ms for at least 1 h) by an array of sixteen 2 × 2 in. NaI(Tl) scintillators. Detectors were located around the column arranged in 4 layers of 4 detectors, symmetrically distributed on the transversal plane and covering a total height of 1 m, as illustrated in the photograph of Fig. 2a. In the case of RPT-AAD, the released tracer motion was continuously followed by an array of fifteen of the same detectors, but located axially aligned along the column. Fig. 2b shows a photograph of the RPT-AAD facility. For the RPT-AAD experiments, the sampling period was adjusted to 10 ms and experiments were again carried out for at least 1 h. For RPT-AAD,

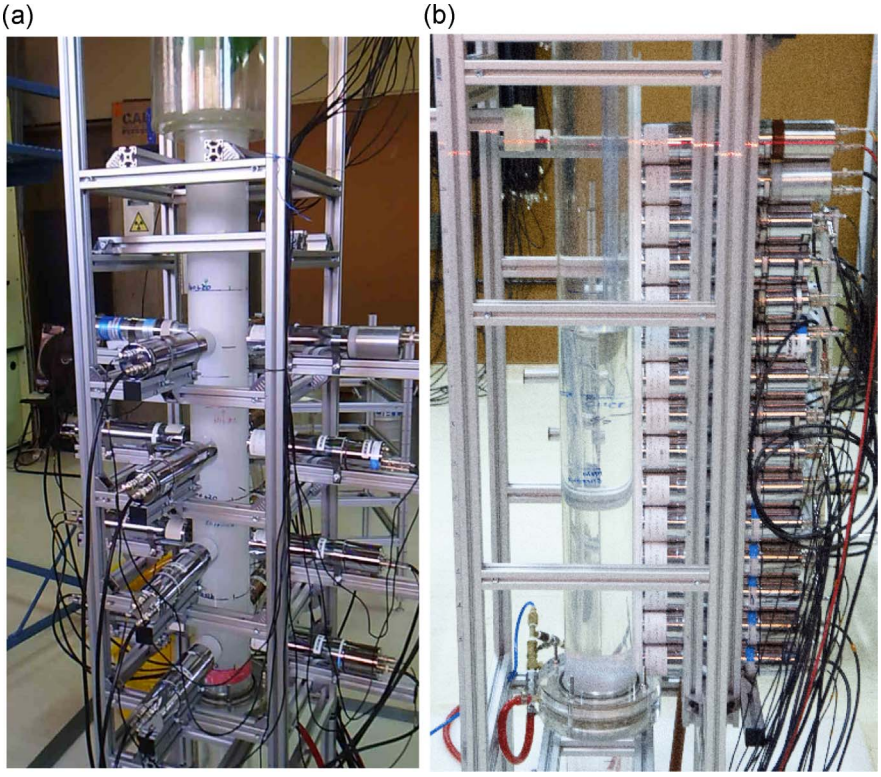

Fig. 2. (a) RPT detection array (left); (b) RPT-AAD detection array (right).

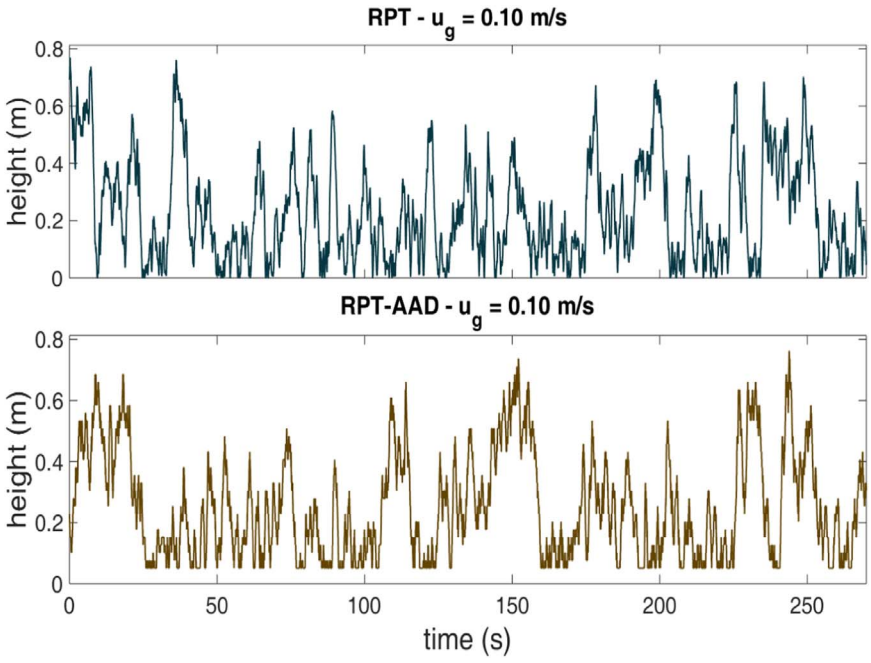

Fig. 3. Comparison of tracer axial trajectories reconstructed from RPT (top) and RPT-AAD (bottom) for the same gas velocity.

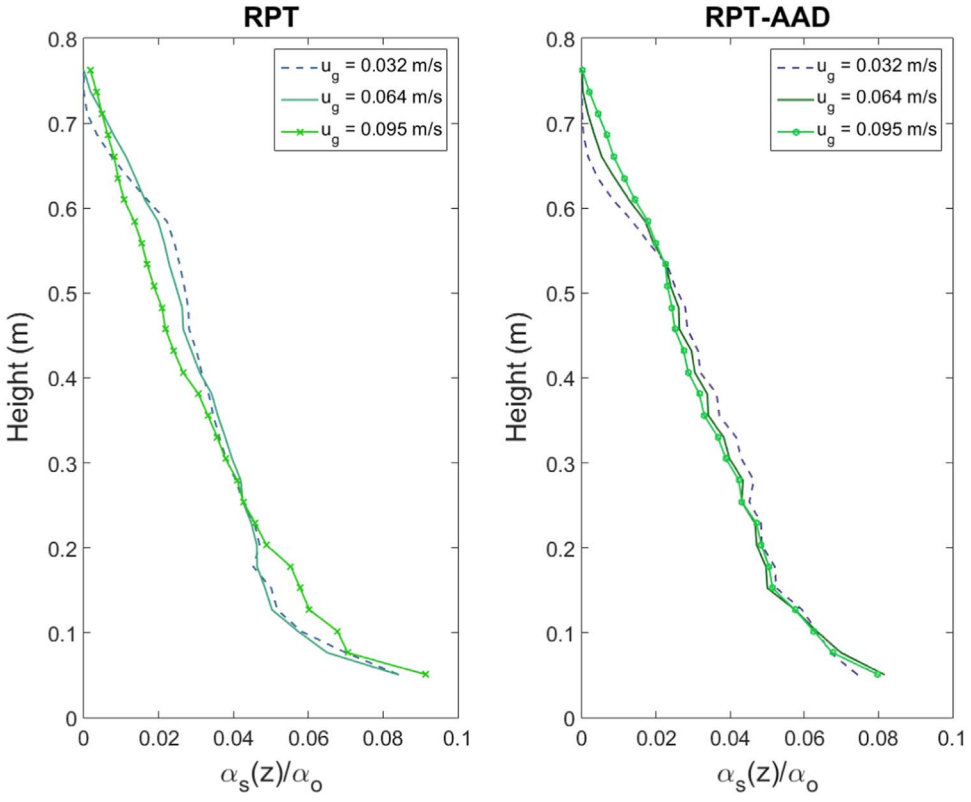

Fig. 4. Axial distribution of the probability of finding the tracer within the column ($\alpha_s(z)/\alpha_0$), determined from trajectories calculated with RPT (left) and RPT-AAD (right) under similar experimental conditions.

since the reconstruction procedure is straight forward, it is less sensitive to statistical noise and more subjected to dynamic bias; then, it is advisable to use a higher sampling frequency. Each scintillation detector was provided with the corresponding photomultiplier and the electronics required for determining the number of photons with energies close to the photopeak of the characteristic γ-rays of the radioisotope used for the experiments.

Additionally, RPT-AAD setup was employed for densitometry measurements. After finishing the RPT and RPT-AAD experiments, the tracer was removed from the vessel and a sealed and collimated external radioactive source (^{241}Am 2 mCi) was located in the opposite side of the column, in front of each detector at a time. The sealed source was moved to align it with each detector axial center and the gamma photons crossing the column were counted with the corresponding detector, for at least the same gas velocities as those explored with RPT and RPT-AAD. With the data, the axial distribution of the chordal gas hold up was obtained.

Trajectory reconstruction procedures used depended on the detectors arrangements. In the case of RPT, tracer positions were determined after estimating each detector response with a model based on Monte

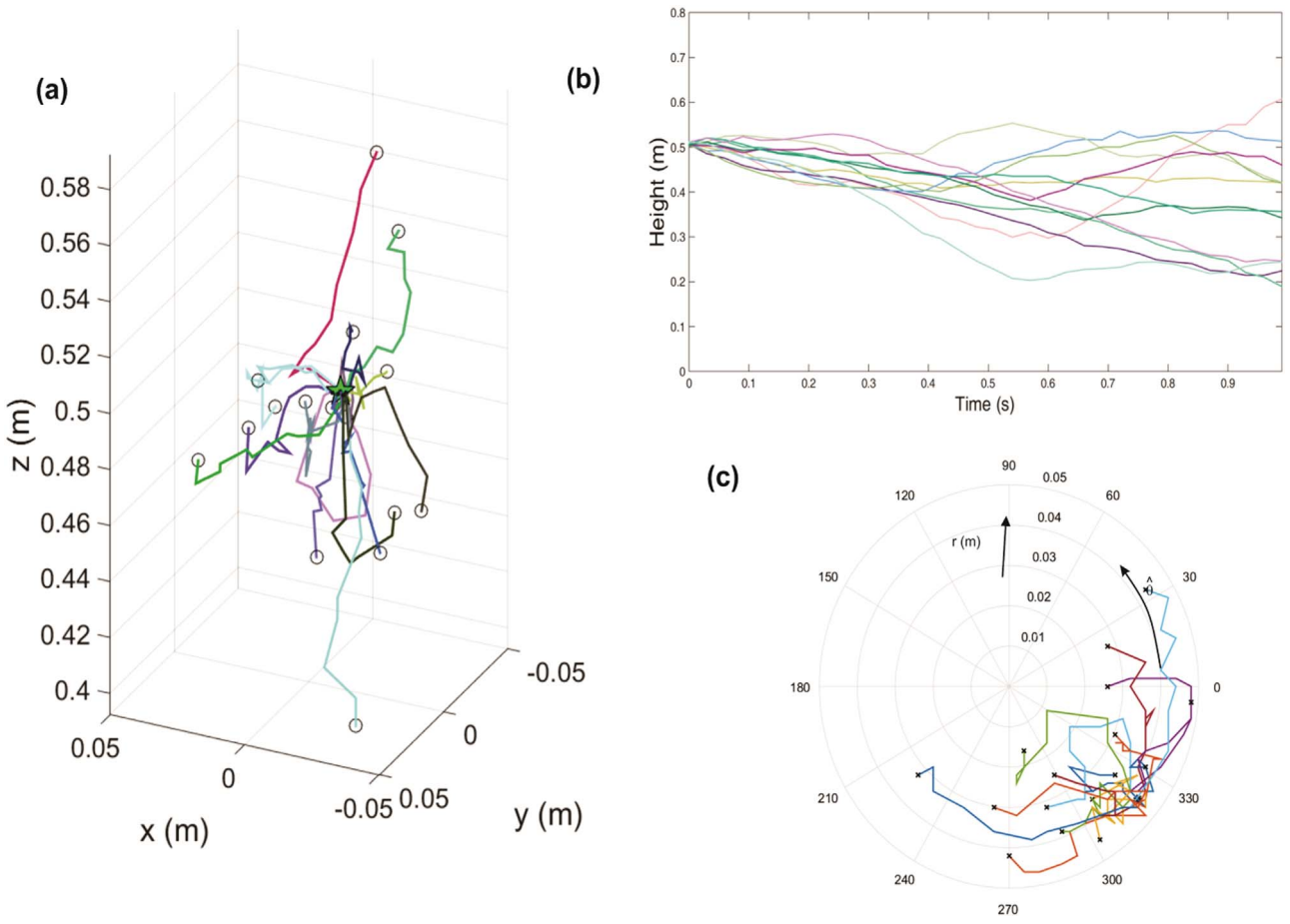

Fig. 5. (a) Manifold of 15 trajectories starting from the same voxel, (b) time evolution of the trajectories axial coordinate, (c) projection of the manifold on the x-y plane.

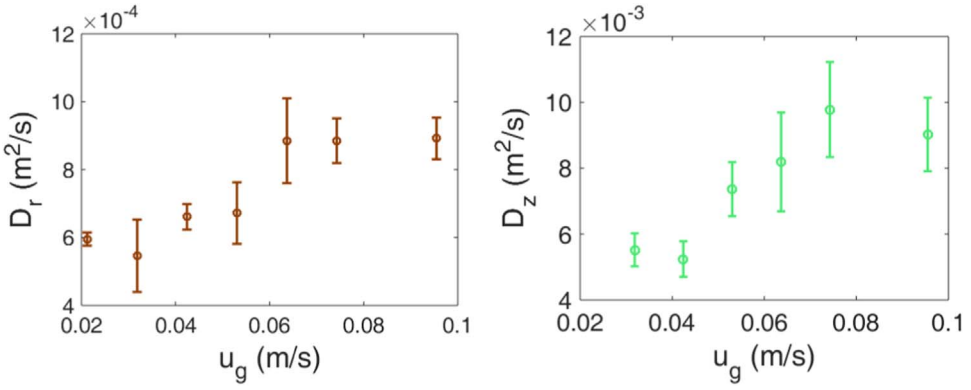

Fig. 6. Solid radial (left) and axial (right) dispersion coefficients determined from RPT as a function of gas velocity.

Carlo. The model parameters, an effective mean attenuation coefficient, the tracer intensity and the detection system dead time, were optimized for each detector by means of a calibration stage. Then, the column was divided in a large number of equal size cells (e.g., ~ 100,000) and the counting of each detector was calculated considering that the tracer was located in each cell. In this way, an estimation of the signal that the 16 detectors would count when the tracer is at many positions inside the column is obtained. This information constitutes a database of correspondence between positions within the reactor and the signal distribution of the detectors arranged around the column [27]. When the tracer is released to freely move within the three-phase emulsion, the "instantaneous" (every 30 ms) tracer positions are estimated by least square minimization of the differences between the measured and estimated counts registered simultaneously by all the detectors in the array.

The reconstruction procedure of RPT-AAD was more straightforward. It involved searching, for each instant (every 10 ms), the detector that measured the highest number of counts. Then, the coordinate of that detector axial center was directly assigned to the tracer axial position for that instant. If two detectors shared a signal with the same order of magnitude (with a 25% tolerance), the assignment was to an axial position located equidistant from the center axis of those detectors. This reconstruction procedure led to a granularity of 2N-1 possible positions (where N is the number of detectors in the axially aligned array). In this case, fifteen detectors were used, totalling 29 possible positions. Further details on the reconstruction procedure can be found in [28]. Naturally, this methodology is particularly suitable for vessels with relatively low diameter and a high aspect ratio (height over diameter), which is typical of many bubble columns at laboratory and pilot scale.

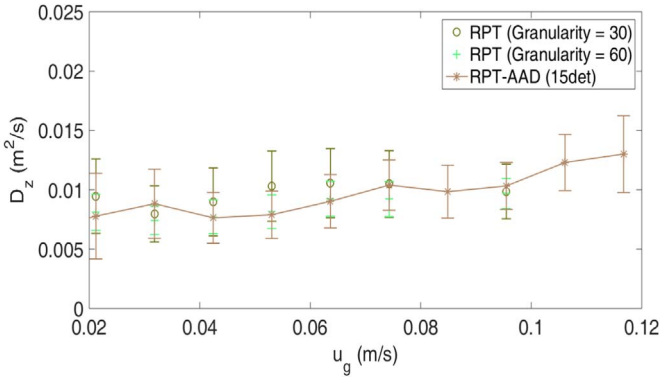

Fig. 7. Solid axial dispersion coefficients determined from RPT-AAD and RPT with two granularities, as a function of gas velocity.

3. Results and discussion

Experiments carried out at the same operating conditions were examined with RPT, RPT-AAD and γ-densitometry. Trajectories determined with both tracking methods, and some information extracted from them, are compared hereafter.

3.1. Tracer trajectories

Typical trajectories of the tracer axial coordinate obtained with RPT and RPT-AAD at similar experimental conditions are shown in Fig. 3 for comparison. As expected, those arising from RPT are slightly more jagged due to the larger granularity of the reconstruction. However, it is important to compare statistics emerging from both, leading to information relevant for design purpose.

3.2. Solid distribution

The first output that can be calculated from the tracer path is the probability of finding the tracer at different locations in the column, which in turn is expected to be related with the local solid holdup [28,29]. The distribution of the solid phase within the column would be a function of the normalized frequency of the tracer occurrences at different voxels. From the distribution, the absolute solid holdup could be recovered considering the mean global solid holdup (α_0). Solid distribution along the axial coordinate can be determined either from the path obtained with RPT or RPT-AAD. Fig. 4 compares the probability of finding the tracer at different axial locations.

Calculated profiles satisfactorily agree in describing the trend of increased solid concentration in the lower region of the column and very limited effect of gas velocity on the axial trend except in the region close to the disengagement zone, as already reported for three phase bubble columns [29,30]. This result points to the ability of RPT-AAD to extract information matching the one inferred from RPT.

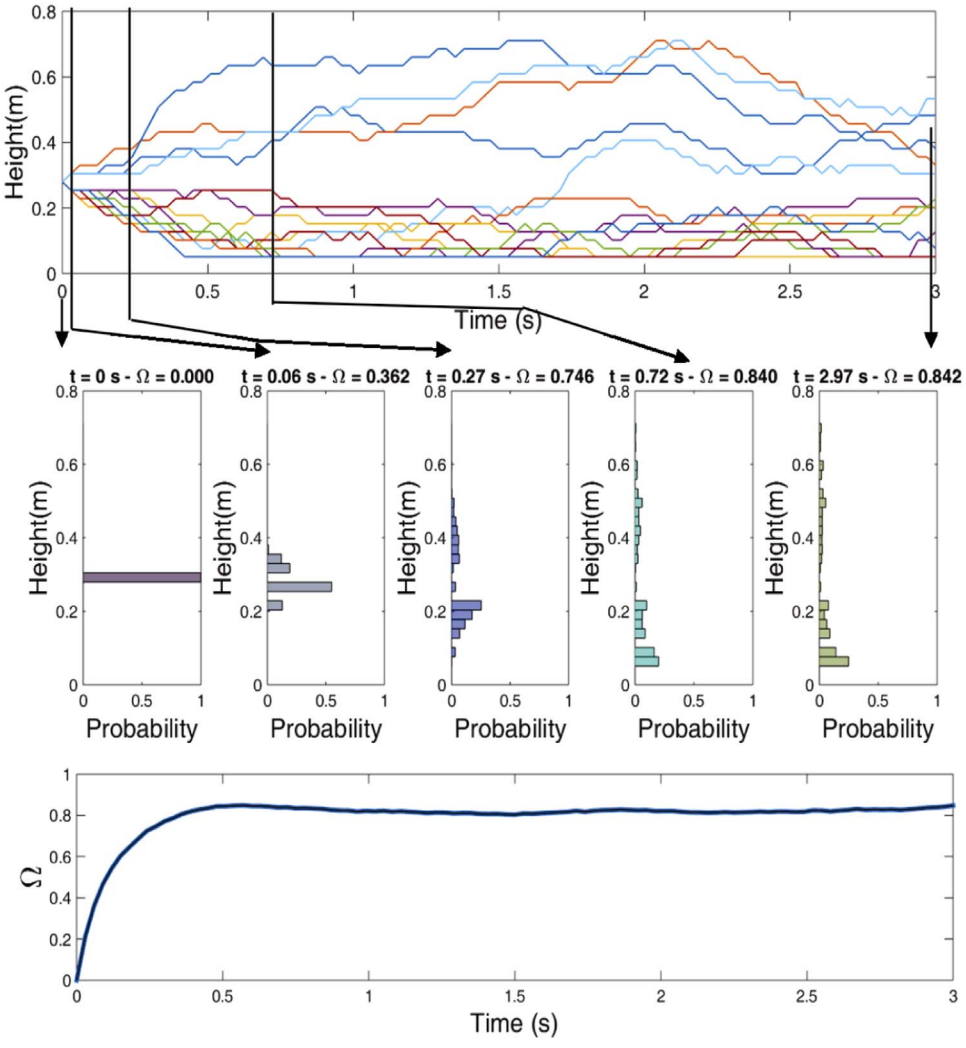

Fig. 8. Manifold of axial trajectories used to calculate the probabilities in Eq. (2) (top). Tracer axial probability distributions for 5 instants after "injection" (middle). Associated normalized entropy (bottom).

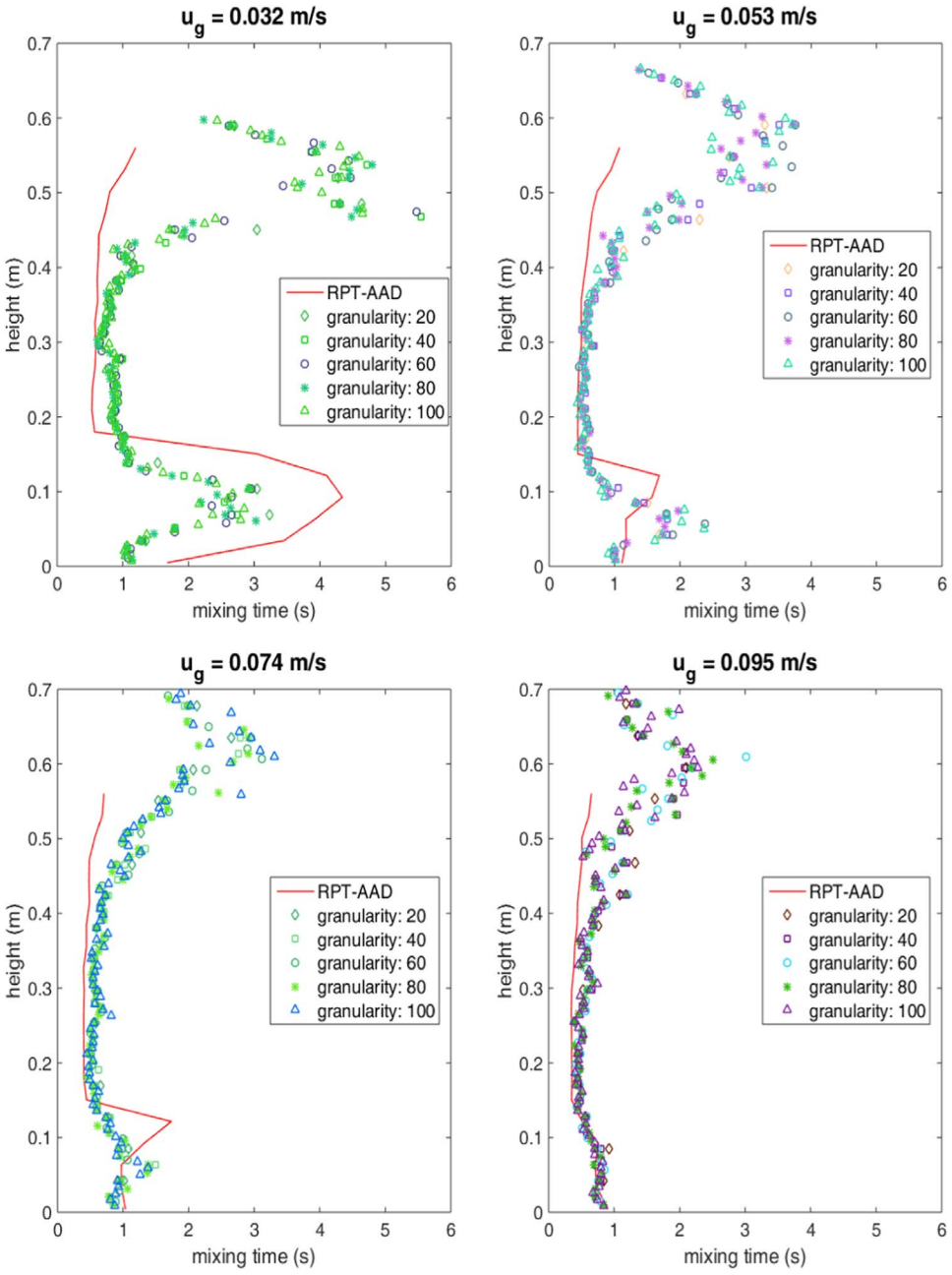

Fig. 9. Solid axial mixing time profile determined from RPT-AAD and RPT with different column discretization (granularity).

3.3. Solid dispersion coefficients

From the prolonged track of the tracer path, which may have more than 300,000 successive positions, extracts at different times starting from a given voxel can be considered to represent different particles based on the hypothesis of ergodicity. Fig. 5 shows a manifold of 15 such trajectories starting from the same voxel.

Extract lengths (~ 5 to 10 s) are defined taking into account the average tracer velocities and the size of the voxel, to capture trajectories that inspect the whole vessel. Correlations are avoided by considering extracts separated at least 10 s in between.

One important parameter frequently used in models for describing the solid motion is the dispersion coefficient (D) of the fluidized particles. This parameter can be estimated considering the relation between the diffusion coefficient and the divergence of molecular paths proposed by Einstein (Eq. (1)), where $\xi^2_{(\tau)}$ is the variance at lag time τ of the paths starting from an initial location ($\overline{x_0}$).

$$D = \frac{1}{2\tau}\xi^2_{(\tau)} = \frac{1}{2\tau}\sum_i (|\overline{x}_{i(\tau)} - \overline{x_0}|)^2 \quad (1)$$

Thus, an estimation of the dispersion coefficient would arise from a linear relationship between the ensemble average of the paths variances centered at the initial point and the lag times. While representing the ensemble-average of the mean square displacements vs the lag time elapsed, a linear trend is apparent once the Lagrange correlation time is exceeded. The linear region generally appeared for time lags of about 1–2 s meanwhile Lagrange correlation time did not surpass 0.1 s.

Radial and axial dispersion coefficients arising from RPT experiments are represented *vs* gas velocity in Fig. 6. Values are calculated considering several initial points at different locations all around the column. The reported values are the average of the local values and the error bar indicates variations among results starting at different positions. Clearly, the influence of gas velocity is larger than the influence of starting point. The positive effect of gas velocity has already been reported in the literature [31,32], as well as the larger values of axial

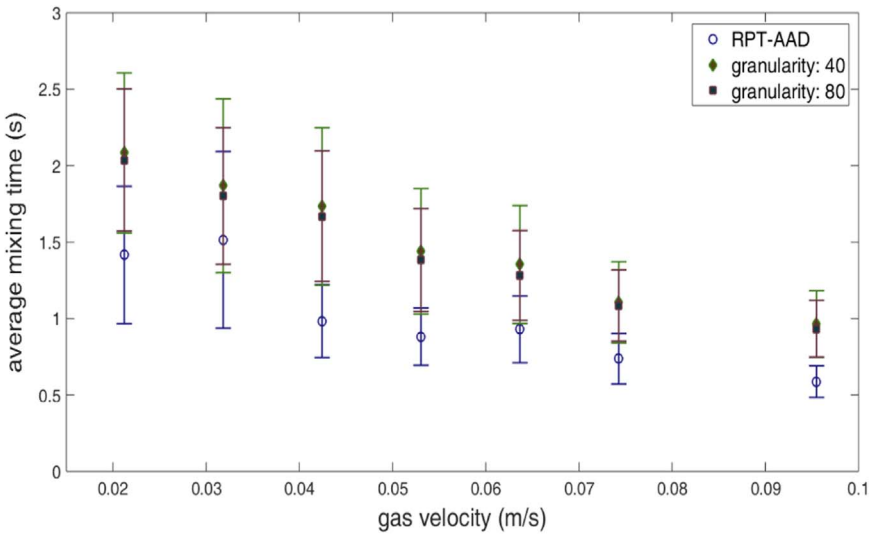

Fig. 10. Solid axial mixing time determined from RPT-AAD and RPT with two granularities, as a function of gas velocity.

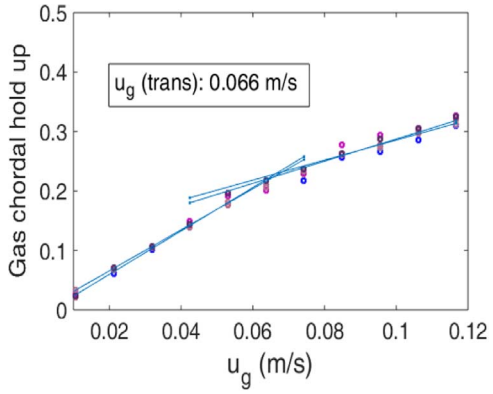

Fig. 11. Chordal gas hold up as a function of gas velocity. Stepwise regression is used for identifying a break in the trend pointing to a flow regime transition.

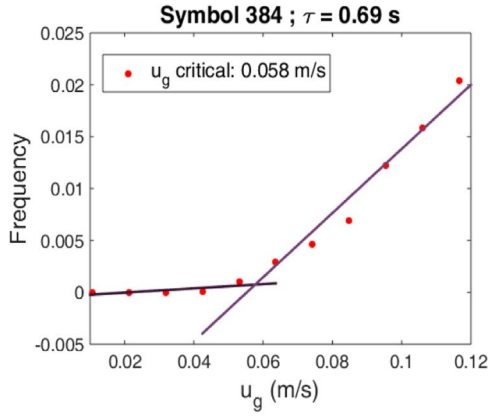

Fig. 12. Frequency of static symbol 384 as a function of gas velocity. Stepwise regression is used for identifying a break in the trend indicating a flow regime transition.

dispersion coefficients compared to the radial ones.

Axial dispersion coefficients can also be calculated from trajectories determined by RPT-AAD. Estimated values of the solid axial dispersion coefficient obtained both from RPT and RPT-AAD are compared in Fig. 7. For RPT, two granularities (number of bins used for space discretization in the axial direction) have been used, to check if the estimated values are sensitive to this parameter; a negligible influence is found considering the variability of the data. For RPT-AAD (15 detectors, i.e., a granularity of 29), results are satisfactorily coincident with those arising from RPT, although the error bars are significantly larger.

3.4. Solid mixing times

The degree of solid mixing can be estimated from the homogeneity achieved by particles released from a given point as time tends to infinity [24,28]. Hence, the normalized information entropy (Eq. (2)) calculated from the space distribution of such particles is used to assess the time required for achieving the asymptotic highest mixing condition. The maximum entropy used for normalization considers a uniform distribution of the particles over the bins or sections used for space discretization.

$$\Omega(t) = -\frac{\sum_{i=1}^{N} [p_{i(t)} \ln(p_{i(t)})]}{\ln(N)} \quad (2)$$

N is the number of bins use for discretization and $p_{i(t)}$ is the probability of finding particles in the ith bin (i = 1,2,…,N). Fig. 8 shows a representative manifold of axial trajectories starting from a given height in the column, and the probabilities calculated from the space distribution of the "released" particles as time passes. The normalized entropy time evolution (Fig. 8 bottom) reaches an asymptotic value lower than 1, related to the maximum level of mixing achievable for the corresponding operating condition. The asymptotic distribution is not completely uniform throughout the bed since the solid phase is slightly denser than the liquid; the asymptotic value achieved depends on the gas velocity.

The time required to reach the asymptotic normalized entropy is considered as an estimation of the axial mixing time. Therefore, axial mixing times have been calculated by taken manifolds of trajectories determined either by RPT-AAD or RPT with similar space discretization (granularity). In addition, for RPT, mixing times have been obtained with several granularities to check if the estimated values are sensitive to the discretization used.

Fig. 9 shows axial mixing time profiles obtained by RPT-AAD and RPT with several granularities, for different gas velocities. Results indicate that the discretization used has a negligible influence on the mixing times calculated with RPT.

Values arising from both methods have similar axial trends in the lower region of the column and indicate that the mixing time depends on gas velocity. For low gas velocities, there is a marked increase in axial mixing time when the solid "injection" location is located close to the emulsion boundaries, particularly around the disengagement zone. Longer times are also necessary to attain mixing when the solid particles are "injected" close to the gas distributor. As gas velocity is

increased, the axial variations are tempered; however, minimum values are always attained around z/D~2–3. Both tracking methods lead to similar values and axial trends, except close to the disengagement region, where the RPT-AAD significantly underestimate the mixing time.

Fig. 10 shows the influence of gas velocity on the average mixing time, calculated as the mean of those obtained from different axial "injection" points. Fairly good agreement is found while comparing the trends obtained from both methods. A negative influence of the gas velocity is found; however, solid axial mixing times calculated from tracer trajectories obtained with RPT are generally longer than those calculated from RPT-AAD.

3.5. Flow regime transitions

The critical velocity of transition between the homogeneous and heterogeneous flow regimes is generally estimated from a break in the trend of gas holdup vs gas velocity. Densitometry experiments carried out to determine chordal holdups are therefore used for this purpose. Fig. 11 expose the influence of gas velocity on chordal holdups calculated from γ-densitometry experiments at different heights around the central region of the column; from about 0.4 to 0.5 m above the gas distributor. The break in the trends is obtained with stepwise regression analysis, and the estimated critical value is given in the figure.

With the aim of diagnosing the transition velocity from RPT-AAD experiments, the combined response of the aligned detectors is analyzed by applying symbolic analysis, to produce quantitative indexes related to the underlying flow regime [33,34]. Therefore, the experimental time series of tracer axial coordinates are converted into a succession of symbols following certain criteria. Afterwards, the symbol sequences are analyzed to search for recurrent patterns and to get fingerprints of the underlying dynamic state. Generally, two approaches are followed, either by defining the symbols from a static or a dynamic viewpoint [33,35]. In this case, we have used the so-called static symbolization.

Static symbolization of the tracer axial coordinate time series implies defining a series of symbols according to the tracer axial location in the bed. The division is arbitrary, the number of regions can be chosen differently; in this case, we decided to define eight equally sized regions. The symbol is built by defining a number 1 to the region where the tracer is located, while the other regions are assigned with a 0. If one instant is considered, only eight binary numbers associated with the detectors position can appear, since the tracer would be at a given position. Hence, to include the influence of the tracer motion, three subsequent instants have been taken, separated with given time lags (τ). Then, symbols obtained can have at most three ones. Even if 2^8 symbols could be defined when eight regions are considered, several symbols never appear (forbidden symbols) since only three instants are "observed". With this procedure, the tracer axial coordinate time series are converted to symbols and the symbol indexes are the decimal representation of the binary numbers. Since the observation windows are generally short (2τ, τ = 0.06–1.5 s), the majority of the symbols contain successive 'ones'. The bottom of the column is associated with the lower exponents while the upper region (close to the disengagement) is indicated by the higher exponents. Then, the frequency of higher numbers is related to the bed expansion, since they indicate the frequency of the tracer in the upper region of the column. Further details on the analysis procedure can be found in [26].

Fig. 12 shows the trend of the symbol 384 (11000000) as the gas velocity is increased. This symbol highlights the appearance of the tracer close to the detectors located in the column top. The striking break observed in the frequency trend has been considered to indicate a flow regime transition. The critical value calculated by stepwise regression is shown in the figure and it is fairly coincident with the value determined from densitometry experiments, a completely independent methodology. This agreement indicates that symbolic analysis of tracer trajectories determined with RPT-AAD can be successfully used to identify flow regime transitions in three-phase bubble columns.

4. Conclusions

The motion of calcium alginate beads induced by gas circulation in a bubble column was noninvasively examined using Radioactive Particle Tracking methods and γ-densitometry. The trajectories and information extracted from a coarse one dimensional reconstruction determined with an array of axially aligned detectors (RPT-AAD) were compared with trajectories obtained with the advanced Radioactive Particle Tracking (RPT) technique. Information extracted fairly agrees, pointing to the capability of the simplified method for estimating some useful parameters. It is particularly important to remark that mixing parameters, like solid axial mixing times and solid axial dispersion coefficients are very well predicted from the simplified method. Moreover, the flow transition inferred from symbolic analysis of RPT-AAD trajectories satisfactorily coincides with the estimation arising from trends of chordal holdups determined by γ-densitometry. Since the simplified method does not require a calibration step, it can be easily applied for monitoring already operating industrial equipment. The simplified method is particularly suitable for high aspect (height over diameter) ratios and it is expected to be less sensitive for high diameter columns.

Acknowledgments

Financial support from FONCyT (PICT2014-0704) and Universidad de Buenos Aires (UBACyT 20020130100544BA) are gratefully acknowledged. G. Salierno, M. Maestri, M. Cassanello, M.A. Cardona and D. Hojman are members of CONICET. We would particularly like to thank the staff of the RA1 reactor of CNEA, Argentina, for the activation of the sources used in this work.

References

[1] M.K. Al Mesfer, A.J. Sultan, M.H. M.H. Al-Dahhan, Study the effect of dense internals on the liquid velocity field and turbulent parameters in bubble column for Fischer–Tropsch (FT) synthesis by using Radioactive Particle Tracking (RPT) technique, Chem. Eng. Sci. 161 (2017) 228–248.
[2] N. Kantarci, F. Borak, K.O. Ulgen, Bubble column reactors, Process Biochem. 40 (2005) 2263–2283.
[3] X. Jia, X. Wang, J. Wen, W. Feng, Y. Jiang, CFD modelling of phenol biodegradation by immobilized Candida tropicalis in a gas–liquid–solid three-phase bubble column, Chem. Eng. J. 157 (2010) 451–465.
[4] R. Krishna, J.M. van Baten, M.I. Urseanu, J. Ellenberger, Design and scale up of a bubble column slurry reactor for Fischer-Tropsch synthesis, Chem. Eng. Sci. 56 (2001) 537–545.
[5] M.P. Dudukovic, P.L. Mills, Scale-up and multiphase reaction engineering, Curr. Opin. Chem. Eng. 9 (2015) 49–58.
[6] H. Pan, X.-Z. Chen, X.-F. Liang, L.-T. Zhu, Z.-H. Luo, CFD simulations of gas–liquid–solid flow in fluidized bed reactors – a review, Powder Technol. 299 (2016) 235–258.
[7] M.C. Gruber, S. Radl, J.G. Khinast, Effect of bubble–particle interaction models on flow predictions in three-phase bubble columns, Chem. Eng. Sci. 146 (2016) 226–243.
[8] S. Roy, Radiotracer and particle tracking methods, modeling and scale-up, AIChE J. 63 (2017) 314–326.
[9] M. Dudukovic, Opaque multiphase flows: experiments and modeling, Exp. Therm. Fluid Sci. 26 (2002) 747–761.
[10] A. Yadav, M. Ramteke, H.J. Pant, S. Roy, Monte Carlo real coded genetic algorithm (MC-RGA) for Radioactive Particle Tracking (RPT) experimentation, AIChE J. 63 (2017) 2850–2863.
[11] M. Vesvikar, M.H. Al-Dahhan, Hydrodynamics investigation of laboratory-scale internal gas-lift loop anaerobic digester using non-invasive CAPRT technique, Biomass Bioenergy 84 (2016) 98–106.
[12] R.K. Upadhyay, S. Roy, Investigation of hydrodynamics of binary fluidized beds via radioactive particle tracking and dual- source densitometry, Can. J. Chem. Eng. 88 (2010) 601–610.
[13] S. Bhusarapu, M.H. Al-Dahhan, M.P. Duduković, Solids flow mapping in a gas–solid riser: mean holdup and velocity fields, Powder Technol. 163 (2006) 98–123.
[14] S. Roy, A. Kemoun, M.H. Al-Dahhan, M.P. Dudukovic, Experimental investigation of the hydrodynamics in a liquid–solid riser, AIChE J. 51 (2005) 802–835.
[15] J. Chen, N. Rados, M.H. Al-Dahhan, M.P. Dudukovic, D. Nguyen, K. Parimi, Particle motion in packed/ebullated beds by CT and CARPT, AIChE J. 47 (2001) 994–1004.
[16] A.R. Rammohan, A. Kemoun, M.H. Al-Dahhan, M.P. Dudukovic, Characterization of single phase flows in stirred tanks via computer automated Radioactive Particle

Tracking (CARPT), Trans. IChemE 79 (2001) 831–844.
[17] S. Degaleesan, M.P. Dudukovic, Y. Pan, Experimental study of gas-induced liquid-flow structures in bubble columns, AIChE J. 47 (2001) 1913–1931.
[18] M. Cassanello, F. Larachi, R. Legros, J. Chaouki, Solids dynamics from experimental trajectory time-series of a single particle motion in gas-spouted beds, Chem. Eng. Sci. 54 (1999) 2545–2554.
[19] K. Kiared, F. Larachi, M. Cassanello, J. Chaouki, Flow structure of the solids in a three-dimensional liquid fluidized bed, Ind. Eng. Chem. Res. 36 (1997) 4695–4704.
[20] N. Devanathan, D. Moslemian, M.P. Dudukovic, Flow mapping in bubble columns using CARPT, Chem. Eng. Sci. 45 (1990) 2285–2291.
[21] F. Larachi, M. Cassanello, J. Chaouki, C. Guy, Flow structure of the solids in a three-dimensional gas–liquid–solid fluidized bed, AIChE J. 42 (1996) 2439–2452.
[22] N. Mostoufi, J. Chaouki, On the axial movement of solids in gas-solid fluidized beds, Trans. IChemE 78 (2000) 911–920.
[23] M. Cassanello, F. Larachi, A. Kemoun, M.H. Al-Dahhan, M.P. Dudukovic, Inferring liquid chaotic dynamics in bubble columns using CARPT, Chem. Eng. Sci. 56 (2001) 6125–6134.
[24] M. Cassanello, F. Larachi, C. Guy, J. Chaouki, Solids mixing in gas-liquid-solid fluidized beds: experiments and modeling, Chem. Eng. Sci. 51 (1996) 2011–2020.
[25] N.E. Holden, Neutron Capture Cross Section Standards for BNL 325, Fourth edition, National Nuclear Data Center, Brookhaven National Laboratory, New York, USA, 1981.
[26] G.L. Salierno, Caracterización de Equipos y Medios Multifásicos con Métodos que Emplean Fuentes Radiactivas, Universidad de Buenos Aires, Argentina, 2016http://digital.bl.fcen.uba.ar/Download/Tesis/Tesis_5951_Salierno.pdf.
[27] J. Chaouki, F. Larachi, M.P. Dudukovic, Non-Invasive Monitoring of Multiphase Flows, Elsevier, Amsterdam, 1997.
[28] G. Salierno, M. Maestri, S. Piovano, M. Cassanello, M.A. Cardona, D. Hojman, H. Somacal, Discrete axial motion of a radioactive tracer reconstructed from the response of axially aligned detectors: application to the analysis of a bubble column dynamics, Chem. Eng. Sci. 100 (2013) 402–412.
[29] S. Grevskott, B.H. Sannaes, M.P. Dudukovic, K.W. Hjarbo, H.F. Svendsen, Liquid circulation, bubble size distributions, and solids movement in two- and three-phase bubble columns, Chem. Eng. Sci. 51 (1996) 1703–1713.
[30] Z.W. Gan, Holdup and velocity profiles of monosized spherical solids in a three-phase bubble column, Chem. Eng. Sci. 94 (2013) 291–301.
[31] K. Kiared, F. Larachi, J. Chaouki, C. Guy, Mean & turbulent particle velocity in the fully developed region of a three-phase fluidized bed, Chem. Eng. Technol. 22 (1999) 683–689.
[32] H.O. Lim, M.J. Seo, Y. Kang, K.W. Jun, Particle fluctuations and dispersion in three-phase fluidized beds with viscous and low surface tension media, Chem. Eng. Sci. 66 (2011) 3234–3242.
[33] C.S. Daw, C.E.A. Finney, E.R. Tracy, A review of symbolic analysis of experimental data, Rev. Sci. Instrum. 74 (2003) 915–930.
[34] V. Rajagopalan, A. Ray, R.R. Samsi, J. Mayer, Pattern identification in dynamical systems via symbolic time series analysis, Pattern Recogn. 40 (2007) 2897–2907.
[35] G. Salierno, M.S. Fraguío, S. Piovano, M. Cassanello, M.A. Cardona, D. Hojman, H. Somacal, Bubble columns dynamics inferred from the motion of a radioactive tracer followed by axially aligned detectors, Chem. Eng. J. 207–208 (2012) 450–461.